# Directed Motion of Colloidal Particles in a Galvanic Microreactor

Linda Jan,[†] Christian Punckt,[†] Boris Khusid,[‡] and Ilhan A. Aksay*,[†]

[†]Department of Chemical and Biological Engineering, Princeton University, Princeton, New Jersey 08544, United States

[‡]Department of Chemical, Biological, and Pharmaceutical Engineering, New Jersey Institute of Technology, University Heights, Newark, New Jersey 07102, United States

Ⓢ Supporting Information

ABSTRACT: The mechanisms leading to the deposition of colloidal particles in a copper–gold galvanic microreactor are investigated. Using in situ current density measurements and particle velocimetry, we establish correlations between the spatial arrangement and the geometry of the electrodes, current density distribution, and particle aggregation behavior. Ionic transport phenomena are responsible for the occurrence of strongly localized high current density at the edges and corners of the copper electrodes at large electrode separation, leading to a preferential aggregation of colloidal particles at the electrode edges. Preferential aggregation appears to be the result of a combination of electrophoretic effects and changes in bulk electrolyte flow patterns. We demonstrate that electrolyte flow is most likely driven by electrochemical potential gradients of reaction products formed during the inhomogeneous copper dissolution.
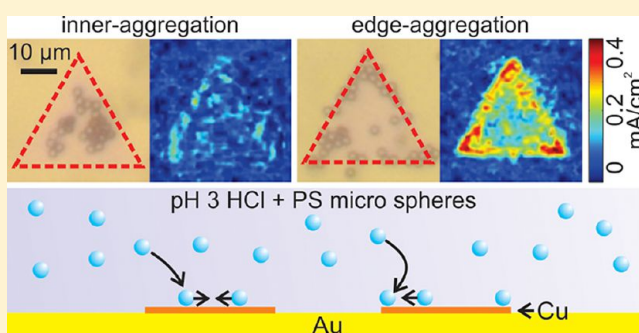
INTRODUCTION

Precise patterning of colloidal single crystals with predetermined orientation is desired for their incorporation into devices including sensors,[1–3] photonic crystals,[4–6] and mesoscopic and hierarchical materials.[7] The use of electrokinetic phenomena has proven to be a versatile approach to guide colloidal aggregation and form patterned colloidal structures due to the possibility to define and control the speed and direction of colloidal particles as well as the location of particle deposition.[8–13] A variety of different techniques has been developed using externally applied electrical fields, including patterned interdigitated electrodes[10,12] or inducing current density heterogeneities on a single electrode through illumination with light patterns,[11] mechanical damage (scratches),[13] or application of insulating surface layers.[9]

Spontaneous electrochemical reactions which are associated with the presence of intrinsic electric fields, such as catalytic decomposition of hydrogen peroxide on pairs of dissimilar metal electrodes[14] or galvanic corrosion,[15] have been used to transport and pattern colloidal particles autonomously without the need for an external power source. Similarly, using a galvanic microreactor system, we recently demonstrated a method capable of autonomously forming complex, predetermined patterns of two-dimensional colloidal single crystals with defined orientation that are cemented to the substrate (Figure 1a and 1b).[15] Our microreactor consisted of an array of galvanic electrodes, anodic copper and cathodic gold, arranged in a coplanar geometry (Figure 1a). When the electrodes came into contact with mildly acidic pH 3 hydrochloric acid (HCl) solution, spontaneous electrochemical reactions occurred on the electrode surfaces:[16–19] In the presence of chloride ions,

dissolution of copper proceeded along different pathways according to[17–19]

$$Cu + 2Cl^- \leftrightharpoons CuCl_2^- + e^- \tag{1}$$

or

$$Cu \leftrightharpoons Cu^{2+} + 2e^- \tag{2}$$

and these reactions were balanced by reduction of dissolved oxygen on the gold cathode[16]

$$O_2 + 2H^+ + 2e^- \leftrightharpoons H_2O_2 \tag{3}$$

Thus, the copper–gold galvanic couple acted as a short-circuited battery, with an ionic current flowing through the electrolyte and an (equal) electronic current flowing through the copper–gold interface. Soluble cuprous chloride complexes[18] formed via eq 1 can further react with water to form cuprous oxide in a subsequent homogeneous reaction[19]

$$2CuCl_2^- + H_2O \leftrightharpoons Cu_2O + 2H^+ + 4Cl^- \tag{4}$$
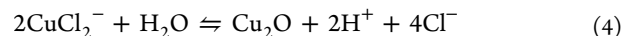
By being "recycled" back into the electrolyte via eq 4, chloride acts similarly to a "catalyst" for copper dissolution and serves as supporting electrolyte.

As the electrochemical reactions proceeded, negatively charged polystyrene (PS) microspheres suspended in the electrolyte moved toward the copper electrodes where they aggregated.[15] We found that the microstructure of the colloidal
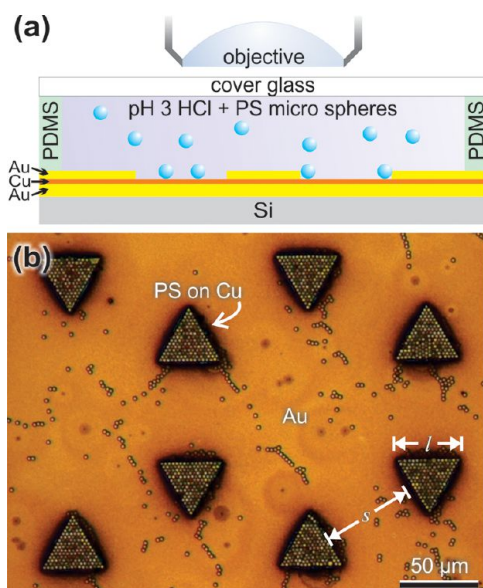
Figure 1. (a) Schematic of the galvanic microreactor (not to scale). Electrodes shown here are of the trench configuration, where the copper surface is lower than the gold surface. PS, polystyrene; PDMS, poly(dimethylsiloxane). (b) Patterned and crystalline two-dimensional colloidal aggregates adherent to triangular copper electrodes imaged after rinsing and drying of the sample. Particles distributed on the gold substrate have been deposited there during rinsing and drying. Parameters: Copper triangle electrodes ($l \approx 40\ \mu m$) with $s \approx 60\ \mu m$ in trench configuration, 0.11 vol % PS particles in pH 3 HCl electrolyte. This electrode geometry exhibits edge-aggregation.

aggregates depended on the location where PS particles aggregated first, and that the location of initial aggregation could be influenced by varying the electrode geometry.[15] When anodic separation s was small ($\approx 20\ \mu m$), PS particles deposited randomly on the inner region of the copper electrode (inner-aggregation) and formed polycrystalline aggregates at the electrode center through electro-osmotic flow (EOF) and electrohydrodynamic (EHD) flow effects.[8,20,21] Conversely, when s was large ($\approx 80\ \mu m$), PS particle aggregation initiated from the corners and edges of the copper electrode (edge-aggregation) where the particles aligned with the raised edges of the gold electrode. Such edge-aggregation was found to be necessary for forming highly ordered particle aggregates as shown in Figure 1b.

We also showed that the long-range particle transport toward the electrodes was primarily influenced by reaction-induced bulk electrolyte flow.[15] This was demonstrated by employing silica microspheres which have a larger density (2.0 g/cm³) than PS (1.1 g/cm³) that undergo sedimentation and therefore, unlike PS particles which either remain suspended in the electrolyte or are attracted to the copper electrodes, can be used to explore colloidal transport near the gold electrode surfaces. Before they settled down on the electrode surfaces, silica particles migrated toward the copper electrode with the same velocity that was observed for PS. However, after sedimenting onto the gold cathodes they reversed direction and migrated away from the nearest copper electrode.[15] Reversal of the silica particles' direction of motion with respect to electric field and ion concentration gradients indicated that long-range particle motion was not due to electrophoresis or diffusiophoresis, in which case the direction of particle motion would be defined solely by electric field, ion concentration

gradients, and particle zeta potential,[15,22,23] but instead the result of bulk fluid flow. However, we did not explain why the spatial patterning of the electrodes affected the directed motion of the colloidal particles resulting in different locations of particle aggregation.

The goal of this paper is to analyze the interplay between spatial patterning of the electrodes, reaction rates (current density), and bulk fluid motion influencing the motion of PS particles resulting in either inner- or edge-aggregation. We first investigate how electrode geometry affects the dissolution current density distribution in situ. On the basis of this analysis, we identify a characteristic current density profile which correlates with edge-aggregation. Through this correlation we determine the potential driving forces for the fluid motion as effected by geometry-dependent electrode kinetics and transport of electroactive species. A numerical simulation is presented to support our arguments.

■ METHODS

A schematic of our experimental setup is shown in Figure 1a. The galvanic mircoreactor consisted of an array of copper anodes surrounded by a continuous gold cathode. To fabricate the electrodes, we first deposited 10 nm of titanium film followed by 100 nm of gold film on a silicon wafer using an e-beam evaporator (Denton DV-502A, Denton Vacuum, Moorestown, NJ). A 20–40 nm copper film was electrolessly plated onto the gold (using a solution of 1.5 g of copper sulfate, 7.0 g of potassium sodium tartrate, 2.0 g of sodium hydroxide, and 5 mL of formaldehyde in 50 mL of deionized (DI) water at 25 °C). On top of the copper, we used standard photolithography to pattern photoresist (AZ(R) 5214-E, Clariant Corp., Somerville, NJ) according to our electrode design. Following photolithography, we formed copper "islands" (copper electrodes raised above the gold electrode) by etching in nitric acid or copper "trenches" (copper electrodes lowered, see Figure 1a) by depositing an additional gold layer on top of the patterned photoresist using the e-beam evaporator and performing a "lift-off". The electrode pattern used for generation of colloidal crystals consisted of identically sized equilateral copper triangles with edge-length l of approximately 38 μm. They were arranged in a "honeycomb" pattern with an alternating apex orientation (and thus parallel edges) and separated by a distance s ranging from 25 to 80 μm as shown in Figure 1b, where the copper electrodes are fully covered by the PS particles. Prior to each experiment, the electrodes were etched for 5 s in pH 3 HCl solution to minimize surface oxide layers. For particle tracking experiments, arrays of copper line electrodes were used.

The reaction cell (Figure 1a) was assembled by placing a 7 mm inner diameter circular poly(dimethylsiloxane) (PDMS) spacer ring of either ≈ 650 or $\approx 1100\ \mu m$ thickness on top of the galvanic electrode substrate. To start the reaction, we filled the chamber with pH 3 HCl solution and enclosed it with a microscope cover glass. For particle aggregation experiments, we suspended surfactant-free sulfate-decorated PS latex particles (lot 53977A, Invitrogen, Eugene, OR) in the electrolyte solution at concentrations between 0.04 and 0.11 vol %. Observations were made with bright-field optical microscopy (Zeiss Axioplan 2, Carl Zeiss MicroImaging, Inc., Thornwood, NY) and recorded using a 12-bit digital CCD camera (Zeiss AxioCam HRc, Carl Zeiss MicroImaging, Inc., Thornwood, NY). The reaction was terminated by opening the cell, rinsing the substrate with DI water, and blow drying with nitrogen.

Tracking experiments with 3.0 μm diameter silica particles (Bangs Laboratories Inc., Fishers, IN) were performed on arrays of 50 μm wide copper line electrodes with $s \approx 310\ \mu m$ in the copper island configuration. Prior to the experiments, silica particles were centrifuged and resuspended in fresh DI water for 3 cycles and diluted to a particle concentration of 0.002–0.005 vol % in pH 3 HCl electrolyte. In situ images of the particles were recorded at 0.5 Hz, and their positions and velocities were analyzed using an algorithm written in house with MATLAB. The centers of tracked particles were

determined using morphological operations. Experiments were conducted with low particle concentrations to avoid particle–particle encounters, and the algorithm removed particles that were so close to one another that they could no longer be differentiated automatically. To decrease the measurement noise, velocities of the particles measured within a spatial interval of ≈ 8 μm were collected and averaged over 20 s. The error bars shown in the tracking data reveal that scattering in the distance and velocity of particles reflect Brownian motion over the time scale of the measurement ($(4D\Delta t)^{1/2}/\Delta t = 0.38$ μm/s).

For dissolution analysis, the topography of copper island electrodes was measured in the manner described by Punckt et al.[24] Color images of the copper thin film were recorded in situ at a frequency of 1 Hz. The color difference between copper thin films of less than 30 nm thickness and the gold substrate is an approximately linear function of the film thickness. Consequently, the time evolution of the topography of the copper film can be determined in situ from the color change of the copper electrodes over time. From the temporal changes in the topography of the copper film, we calculated the dissolution rate (measured in nm/s) and corresponding current density distribution on the anodic copper surface, assuming that copper dissolution takes place through a one-electron process that involves a cuprous chloride complex (see eq 1).[17−19] This leads us to a lower limit for the actual current density since to a certain degree also two-electron processes occur during copper dissolution. To decrease measurement noise, color data were averaged over several images taken during a period of 5 s. Current density measurements could not be performed on the cathode in this manner as color changes there are not related to Faradaic current but rather to deposition of reaction products.[24]

The electrophoretic mobility of PS and silica particles suspended in pH 3 HCl electrolyte was obtained using a Coulter DELSA 440SX unit (Beckman Coulter, Inc., Miami, FL). Measurements of mobilities of PS particles were taken at 11 different positions across a rectangular capillary cell using three detection angles. Particle motilities were found to give an excellent fit to the Komagata equation ($R^2 = 0.99$ for all detection angles), which was used to determine electrophoretic mobility.[25] The motilities were averaged over all detection angles for two profile runs. The method of O'Brien and White[26] was used to calculate the particle zeta potential from the measured electrophoretic mobility. We neglected surface conductance because of the relatively low ionic strength (1 mM) of our system. PS particles in pH 3 HCl solution had a zeta potential of -44 ± 3 mV. Profile measurements could not be conducted with the silica particles because they settled over the time required to collect a full profile (≈ 45 min). Thus, we measured the particle mobility only in a single stationary plane using 14 samples and three detection angles. The zeta potential of the silica particles was measured to be -39 ± 4 mV.

To estimate the geometry of flow cells numerically, we determined the steady-state solution of the incompressible Navier–Stokes equations at low Reynolds number in a 500×500 μm^2 system with no slip boundary condition at the top and periodic boundary conditions on the side walls using COMSOL. On the bottom boundary, the profile of a fluid slip velocity was defined based on the current density distribution over the copper and gold electrodes (see below).

■ RESULTS AND DISCUSSION

In the following sections, we first investigate the effect of electrode geometry on the Faradaic current density distribution, reaction kinetics, and ion transport. We focus our observations on the copper anode and location of PS aggregation and show that the current density is influenced by three factors: (i) available cathodic surface area (due to kinetically limited cathode reactions, which include reduction of dissolved oxygen into hydrogen peroxide[16,27]), (ii) ionic transport, and (iii) concentration effects.

Effect of Electrode Geometry on the Current Density Distribution. Figure 2 shows anodic current density
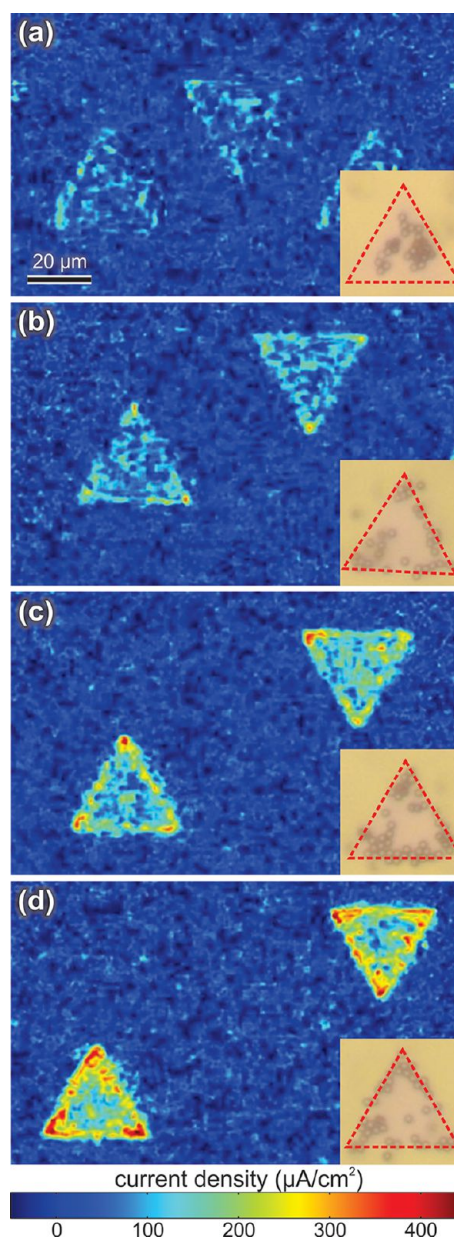

current density (μA/cm^2)

Figure 2. Initial ($t \approx 10$ s) current density distribution as calculated from the dynamic copper dissolution profile on identically sized copper triangle islands ($l \approx 35$ μm) for different anodic separation distances s: $s \approx$ (a) 25, (b) 40, (c) 60, and (d) 80 μm. (Insets) In situ optical images of PS aggregation on copper electrodes: (a) inner-aggregation and (b)−(d) edge-aggregation are observed. Dashed lines indicate the boundaries of the underlying copper electrode.

distributions as a function of electrode spacing s measured about 10 s after initiation of the reactions. Values for s were chosen such that we observe inner-aggregation of PS particles on electrodes with the smallest s (Figure 2a), a mix of inner- and edge-aggregation for $s \approx 40$ μm (Figure 2b), and edge-aggregation for all larger values of s (Figure 2c and 2d). The measured current density increases with s. At $s \approx 80$ μm, along the electrode edges, particularly at the corners, values of ≈ 450 μA/cm^2 are reached, while at the electrode centers, lower currents between 100 and 250 μA/cm^2 are observed (Figure 2d). For smaller values of s, the current density profiles remain heterogeneous but the overall magnitude decreases. At $s \approx 25$ μm, the current density at the electrode edges is only slightly

larger than the measurement noise level (<100 μA/cm^2) such that spatial features in the current density cannot be resolved (Figure 2a). In summary, the results show that edge-aggregation of PS particles occurs in the presence of locally high and heterogeneous current density.

The factors leading to variations in current density can be easily understood: Since the dissolution of copper is catalyzed by the presence of chloride ions,[19] the overall reaction is limited by the slow rate of oxygen reduction on the gold cathode[27] and therefore by the total available gold surface area.[28] As we reduce the spacing of the copper electrodes, we decrease the available cathodic surface area and thus reduce the overall reaction rate. However, by varying s, we not only change the cathodic surface area but also alter the copper area coverage $\theta_{Cu} = A_{Cu}/A_{total}$, i.e., the ratio of the copper to electrolyte volume, which changes the average concentration of reaction products and thus affects electrochemical equilibria and reaction rates. Furthermore, variations in anode spacing affect the transport of ions away from the high current density areas on copper, as can be understood by considering the solution of Laplace's equation for ion diffusion in systems of different geometry.[29] Lastly, ionic (as well as electronic) currents are distributed in the microreactor such that energy dissipation is minimized. In the case of a kinetically limited reaction, such as oxygen reduction on the gold, the charge transfer reaction itself (eq 3) is associated with a high so-called charge transfer resistance (also known as polarization resistance, kinetic resistance, chemical resistance),[22,30,31] and consequently, the ionic current spreads out over the majority of the cathode. In order to determine the contribution of variations in gold surface area to the observed changes in current density independent from contributions of changes in ionic transport and accumulation effects near the copper anodes, we conducted experiments in which we altered the exposed cathodic surface area with photoresist coatings, as detailed in the following.

Kinetic Limitations vs Transport and Concentration Effects. By partially blocking the cathode with an insulating layer of photoresist, we can keep the ratio of the active gold and copper areas $R = A_{Au}/A_{Cu}$ constant while varying the copper surface area fraction θ_{Cu} (with respect to total geometric surface area). The photoresist-modified electrode with $s \approx 80$ μm shown in Figure 3 is characterized by $R \approx 4$ and $\theta_{Cu} \approx 0.04$. As shown in Figure 3b, we obtain a heterogeneous current distribution and observe that the current density on the photoresist-modified electrode reaches about 250 μA/cm^2 at the electrode edges. In the photoresist-modified system, PS particles start aggregating along the edges and corners of the copper electrodes (Figure 3c), likely because this state exhibits similar current density and heterogeneity as observed for the pristine electrode with $s \approx 40$ μm where edge-aggregation is observed as well (Figure 2b). The current density on the photoresist-modified electrode has a significantly larger value than that obtained on the nonmodified electrode with $s \approx 25$ μm shown in Figure 2a which exhibits the same value of $R \approx 4$ (i.e., identical accessible gold surface area) but a 5 times larger copper surface area fraction ($\theta_{Cu} \approx 0.2$, i.e., larger accessible electrolyte volume). Therefore, in the case of small electrode spacing (Figure 2a) dissolution of copper is limited not only by the comparably small cathodic surface area but also by the decreased rate of transport and thus by the accumulation of reaction products generated on the anode in a comparably small volume of electrolyte. This accumulation shifts the equilibrium potential for the dissolution reaction to a more
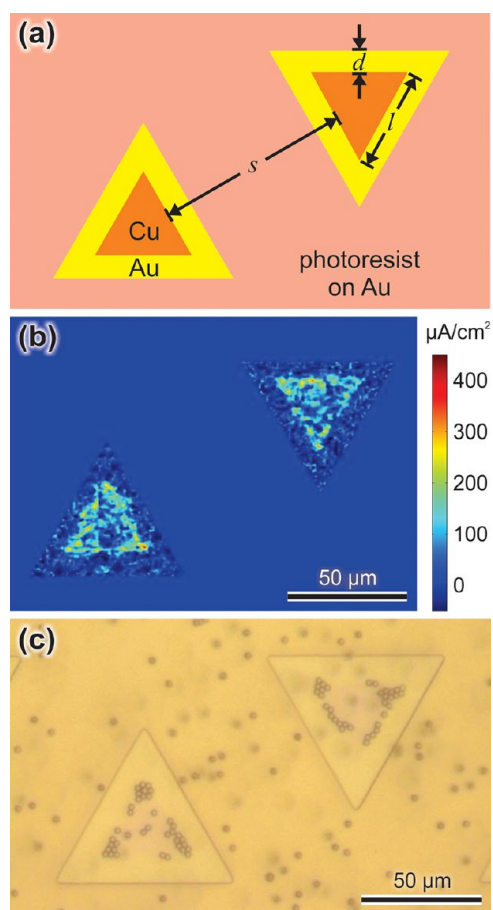

Figure 3. Experiments with photoresist-modified electrodes. Photoresist partially covers the gold surface, reducing active gold surface area exposed to the electrolyte. (a) Schematic of a photoresist-modified electrode. We choose to examine identically sized copper triangles ($l \approx 35$ μm) with the large anodic separation ($s \approx 80$ μm), where in the pristine case edge-aggregation is observed. Thin layer of photoresist blocks off most of the gold such that only a strip of width $d \approx 11$ μm immediate to the copper electrode is exposed. (b) Initial current density distribution ($t \approx 12$ s) on the photoresist-modified electrode system. Reducing active gold area suppresses the current density magnitude compared to the pristine electrode of the same geometry. (c) PS aggregation initiates from the edges and corners of the copper anodes in the photoresist-modified electrode system.

positive value according to the Nernst equation.[32] The electrochemical overpotential which drives the dissolution reaction decreases, and the reaction rate drops. Conversely, decreasing θ_{Cu} effects improved ionic transport and decreased concentration of anodic reaction products (due to comparably large electrolyte volume) which shifts the equilibria of the anodic reactions toward increased copper dissolution. Comparing the current densities of the photoresist-modified electrode with the pristine $s \approx 80$ μm electrode (Figure 2d), where s and θ_{Cu} are the same but R in the pristine electrode is higher (≈ 24), we find that the current density of the photoresist-modified electrode is lower. This illustrates that a decrease in available cathodic area reduces the current since it no longer can spread out over a sufficiently large surface to sustain the electrochemical reaction rates that can potentially be achieved at the anode in this geometry.[27] The photoresist-modified electrode thus appears to represent a case where the reaction rate is affected both by the limited rate of oxygen reduction and by

accumulation of reaction products in the electrolyte slowing copper dissolution.

These findings are further supported by calculating the diffusion-limited current for different electrode geometries. Using the diffusion constant of the slowest species involved in the anodic reactions $D_{CuCl_2^-} \approx 5.7 \times 10^{-10}$ m^2/s and a typical anodic reactant concentration of approximately 1 mM (pH 3 HCl solution has, in very good approximation, a concentration of 1 mM), the one-dimensional diffusion limited current density (Cottrell) at 10 s is ≈ 40 μA/cm^2.[31,33] For the $s \approx 25$ μm electrode array, diffusive transport can be approximated as one-dimensional because s is small compared to the diffusion layer thickness ($\delta|_{t \approx 10\,s} \approx 130$ μm) and the initially hemi-spherical diffusion layers of the individual copper anodes overlap within a few seconds creating an effectively one-dimensional concentration profile for all ionic species involved.[29] Consequently, the observed current density of about 50 μA/cm^2 lies near the calculated Cottrell current density. The current density of up to 450 μA/cm^2 measured for $s \approx 80$ μm in the absence of photoresist, on the other hand, comes close to the limiting current that can be calculated for hemispherical diffusion (600 μA/cm^2 on 10 s time scale).[34] In this case, hemispherical diffusion describes the transport within the reactor more accurately, because during a large fraction of the observation time the developing hemispherical concentration profiles around each copper anode do not overlap with those of neighboring electrodes.[34] In the presence of photoresist, such large current densities cannot be achieved due to the surface area of the cathode being insufficient to sustain the necessary high rate of oxygen reduction.

It is a well-established concept in electrochemistry that spatial variations of the electrochemical reaction rate are small if the reaction under consideration exhibits a large charge transfer resistance, i.e., if large overpotentials are necessary to drive the reaction (secondary current distribution on a highly polarizable electrode).[30,31] This effect is, for example, used during electrodeposition of metals where, by addition of surfactants which partly block the electrode, the charge transfer resistance is increased in order to achieve a more homogeneous coating. To repeat, these conditions are met on the gold cathode. On the copper anodes, on the other hand, due to chloride complex formation, dissolution of copper is a fast process and therefore controlled by ionic transport (primary and tertiary current distributions),[30,31] resulting in strong current density heterogeneities. Diffusion due to increased access to the electrolyte at the copper electrode edges and corners contributes the locally increased current densities there as compared to the electrode center where diffusion can be approximated as one dimensional. The observed current density heterogeneity due to both diffusion- and migration-related effects likely becomes more pronounced as s increases due to increased electrolyte volume between the anodes and lesser amounts of accumulating reaction products, amplifying differences in the (small) Ohmic drop between different locations on the electrodes. Unfortunately, the noise level of our current density data does not allow for experimental verification of this hypothesis. Temporal analysis of dissolution rate and particle motion as done below, however, provides additional evidence for the importance of concentration and ionic transport effects.

Analysis of Temporal Behavior: Further Evidence for Transport and Concentration Effects. The current density profiles for a copper line electrode array shown in Figure 4a
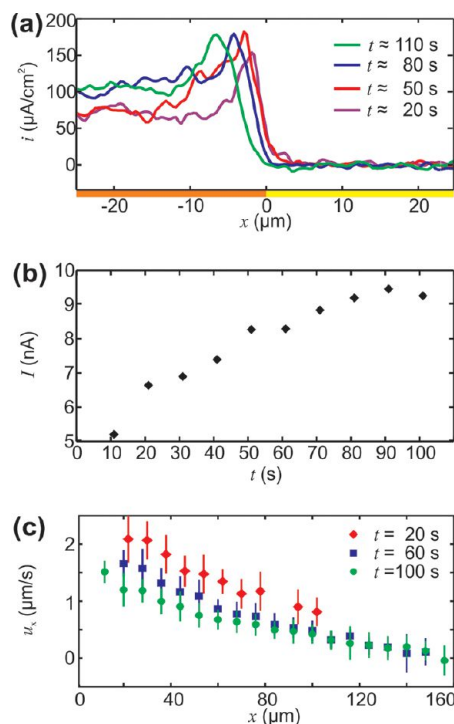

Figure 4. For an array of line electrodes ($l \approx 50$ μm, $s \approx 310$ μm): (a) current density over one-half a copper electrode located at -25 μm $\leq x \leq 0$ μm where $x \approx -25$ μm is the copper electrode center. (b) Total current density (nA) over a copper electrode area of ≈ 8300 μm^2 as a function of time t. (c) Tracking of the lateral velocity of silica particles for different time intervals on the gold electrode surface located at $x \geq 0$ μm as they move away from the copper and gold interface at $x \approx 0$ μm.

reveal that the current density heterogeneity decreases in time. The high current zone near the copper edge ($x \approx 0$ μm) broadens, and while the value of the maximum current density at the edge remains approximately constant, the current density at the electrode center ($x \approx -25$ μm) increases. At the same time, the total (integral) current increases in time (Figure 4b). The location of the current density maximum slightly shifts toward the center of the copper electrode. We attribute the smoothening of the current profile over time to the aforementioned concentration changes in the electrolyte: accumulation of soluble reaction products in the electrolyte, including $CuCl_2^-$ and Cu^{2+},[16-19] increases the electrolyte conductivity, which results in increased ionic currents further away from the copper−gold interface, thus increasing the dissolution rate near the electrode center. At the same time, the reaction equilibrium at the edge of the copper electrode is shifted toward decreased dissolution rate, limiting copper dissolution at later stages of the experiment. The shift of the maximum current toward the electrode center can be attributed to a slight decrease in electrode width as the gold underneath the copper electrode gradually becomes exposed, but may also be partially caused by a concentration-induced attenuation of the dissolution reaction at the copper−gold interface.

During electrode dissolution, the velocity of silica particles on the gold electrode moving away from copper lines decreases in time despite increased overall current (Figure 4c). Because of the moderately large electrolyte conductivity of 400 μS/cm and low ionic current densities of less than 0.5 mA/cm^2, electrophoresis does not contribute significantly to the long-

range motion of PS and silica particles (see Supporting Information for reproduction of evidence and argument for bulk fluid motion).[15] Therefore, the decreasing velocity of silica particles is associated with a decrease in fluid flow along the surface of the gold electrode, and this observation is correlated with the smoothening of the dissolution rate profile. In other words, we find that bulk fluid flow in our reactor and consequently the velocity of silica particles on the gold cathode are dependent on the gradient of the copper dissolution rate.

Related results of numerical simulations have been reported in the literature recently: Moran and Posner have shown that reaction-induced charge autoelectrophoretic fluid motion can decrease with increasing electrolyte conductivity which may increase in time in the microreactor.[35] As the composition and conductivity of the electrolyte change, reaction products, such as cuprous oxide,[15,19] can deposit on the electrodes, altering their native surface charge. All of these effects may affect electrokinetic fluid motion but can currently not be evaluated experimentally.

Preferential Particle Aggregation as Effected by Electrophoresis and Fluid Flow. Near or on the copper electrodes, particularly at the high current edges, electrophoresis may be responsible for directly pinning the particles and thus prevent them from being recirculated into the electrolyte by fluid motion. This local electrophoretic effect increases in magnitude as the current density increases. Thus, one explanation for the occurrence of edge-aggregation at large electrode spacing is the increased contribution of electrophoretic attraction toward high current areas. As we will show in the following, however, also bulk fluid flow has an effect on the location of particle deposition.

To illustrate possible geometries of flow cells and how they can affect the location of particle deposition, we take into account that the bulk fluid motion in the galvanic microreactor is primarily driven by the gradient of the electrochemical potential μ of the cuprous chloride complex above the anode (i.e., at the outer boundary of the diffuse layer) and can be expressed in terms of the fluid slip velocity $u_{slip} \sim \nabla_s \mu$. This assumption is based on theories for an electrochemical cell in a binary electrolyte,[36,37] which showed that the effects of the spatial variation of ion concentrations on the fluid flow can be expressed in terms of the fluid slip velocity. Physically, formation of such flows is caused by the tendency of the system to equilibrate. Thus, their presence can be postulated based on the most basic principles of thermodynamics. In the galvanic microreactor, spatial variations of ion concentrations are certainly present due to the microreactor's coplanar electrode configuration, in particular when current density distributions are heterogeneous. We assume that the flow generated over the copper electrode to equilibrate these heterogeneities dominates, because the current density heterogeneity is more prominent on copper compared to gold (see above). On the copper electrode, the most relevant counterion to consider is the cuprous chloride complex since it is the slowest diffusing species in the microreactor. The concentration of the cuprous chloride complex is related to its rate of formation via Fick's law, and because the diffusion length is short at the early stage of our experiments, the cuprous chloride complex concentration and its rate of formation are roughly proportional. As an approximation for the spatial profile of μ, we thus employ the current density distribution as determined on the copper line electrodes (Figure 4a). Using this assumption, we calculated the fluid flow

within our microreactor by assigning a spatially varying slip velocity to the copper surfaces: $u_{slip} \sim \nabla_s i$.

In Figure 5, we show the computed flow pattern driven by a fluid slip velocity u_{slip} over a pair of galvanic electrodes as
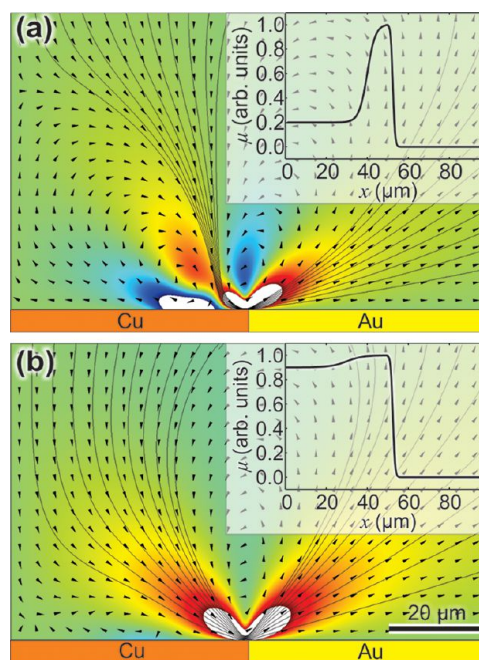

Figure 5. Calculations of the fluid flow pattern driven by electrochemical potential gradients near the copper−gold junction. (a) Presence of two counter-rotating flow cells due to a strongly localized maximum of the electrochemical potential near the electrode interface. (b) Dominance of one flow cell due to a more homogeneous electrochemical potential on the copper electrode. Images show only a part of the complete 500×500 μm^2 system. (Insets) Fluid slip velocity on and near the copper electrode is assumed to follow current density measurements for large (a) and small (b) electrode spacing (Figure 4a). Left boundary of the flow images corresponds to $x = 0$ μm.

numerically calculated from two electrochemical potential profiles with different degree of heterogeneity (see Figure 5 insets). We find that the steep outer gradient in the current density profile drives fluid motion *away* from copper extending over the gold surface, which is consistent with our observed motion of the silica particles on gold. The recirculation of this large flow cell likely brings particles, such as PS, suspended above the electrode surface toward the copper electrode, which is also consistent with our observations. The decrease in current density (and therefore in electrochemical potential) toward the center of the copper electrode drives another, counter-rotating flow cell directly over the copper surface. When the inner rotating flow cell is strong compared to the outer one, as shown in Figure 5a, PS particles located above the copper electrode can likely be directed toward the electrode edge before they reach a distance close to the electrode surface where they would become entrained by electrophoresis. When the counter-rotating flow is weak, as shown in Figure 5b, it is not effective in directing particles toward the edge before they reach the vicinity of the electrode where electrophoresis dominates. Thus, particles are more likely to deposit randomly over the inner region of the copper electrodes and later crystallize at the electrode center by EOF and EHD flow,[8,20,21] resulting in inner-aggregation.

■ SUMMARY

We showed that the motion and the aggregation behavior of colloidal particles in a galvanic copper–gold microreactor are under a mixed control of cathode kinetics and anodic diffusive transport. The edge-aggregation of polystyrene (PS) particles at large copper electrode separation s is correlated with high current density at the corners and edges of the electrodes. Conversely, inner-aggregation at small s is associated with low current density. Experiments conducted by partially blocking the cathode with photoresist revealed that the increase in current density magnitude with s is due to both an increase in the kinetically limited cathodic reaction rate caused by the increase in gold to copper area ratio as well as enhanced transport of anodic reactive species, primarily by diffusion, as the copper separation increases.

We hypothesize that fluid flow is driven to attenuate surface variations of the electrochemical potential of ions μ along the electrode. These are caused by heterogeneous current densities at the copper edge whose effects are expressed in terms of the fluid slip velocity that follows the current density distribution along the copper electrodes. The flow pattern computed based on this hypothesis is found to be consistent with the experimentally observed long-range trajectory of both PS and silica particles. The degree of heterogeneity of the electrochemical potential affects the flow pattern and, consequently, location of particle deposition: When the electrochemical potential profile over copper is highly heterogeneous (which may occur at large s), fluid flow can direct PS toward the copper edges. When the electrochemical potential profile is more homogeneous, a likely scenario at small s, particles deposit randomly over the inner region of the copper electrode. While our calculations provide a possible explanation of inner- versus edge-aggregation in the galvanic microreactor as affected by spatial patterning of the electrodes, a challenge remains to develop an analytical solution for fluid motion over reacting surfaces in a multicomponent electrolyte, where sufficiently large current densities are exhibited and, consequently, concentration gradients can be considered in order to account for our experimentally observed difference in particle trajectories. Such analytical solution would be useful for guiding the deposition and aggregation of colloidal particles in the galvanic microreactor toward precise patterning of colloids and toward development of an adaptive, self-healing material where autonomous accumulation of matter at a precise location is required in response to external stimuli (e.g., corrosion).

■ ASSOCIATED CONTENT

Ⓢ Supporting Information

Calculations supporting arguments concerning electrokinetic effects (electrophoresis, dielectrophoresis, and diffusiophoresis). This material is available free of charge via the Internet at http://pubs.acs.org.

■ AUTHOR INFORMATION

Corresponding Author

*E-mail: iaksay@princeton.edu.

Notes

The authors declare no competing financial interest.

■ ACKNOWLEDGMENTS

■ ABBREVIATIONS

DI, deionized; EOF, electroosmotic flow; EHD, electrohydrodynamic; PDMS, poly(dimethylsiloxane); PS, polystyrene

■ REFERENCES

(1) Holtz, J. H.; Asher, S. A. Nature 1997, 389, 829−832.
(2) Baksh, M. M.; Jaros, M.; Groves, J. T. Nature 2004, 427, 139−141.
(3) Ben-Moshe, M.; Alexeev, V. L.; Asher, S. A. Anal. Chem. 2006, 78, 5149−5157.
(4) Vlasov, Y. A.; Bo, X. Z.; Sturm, J. C.; Norris, D. J. Nature 2001, 414, 289−293.
(5) Cui, Y.; Bjork, M. T.; Liddle, J. A.; Sonnichsen, C.; Boussert, B.; Alivisatos, A. P. Nano Lett. 2004, 4, 1093−1098.
(6) Rinne, S. A.; Garcia-Santamaria, F.; Braun, P. V. Nat. Photonics 2008, 2, 52−56.
(7) Dionigi, C.; Stoliar, P.; Ruani, G.; Quiroga, S. D.; Facchini, M.; Biscarini, F. J. Mater. Chem. 2007, 17, 3681−3686.
(8) Trau, M.; Saville, D. A.; Aksay, I. A. Science 1996, 272, 706−709.
(9) Yeh, S. R.; Seul, M.; Shraiman, B. I. Nature 1997, 386, 57−59.
(10) Ramos, A.; Morgan, H.; Green, N. G.; Castellanos, A. J. Phys. D, Appl. Phys. 1998, 31, 2338−2353.
(11) Hayward, R. C.; Saville, D. A.; Aksay, I. A. Nature 2000, 404, 56−59.
(12) Velev, O. D.; Bhatt, K. H. Soft Matter 2006, 2, 738−750.
(13) Ristenpart, W. D.; Jiang, P.; Slowik, M. A.; Punckt, C.; Saville, D. A.; Aksay, I. A. Langmuir 2008, 24, 12172−12180.
(14) Kline, T. R.; Iwata, J.; Lammert, P. E.; Mallouk, T. E.; Sen, A.; Velegol, D. J. Phys. Chem. B 2006, 110, 24513−24521.
(15) Punckt, C.; Jan, L.; Jiang, P.; Frewen, T. A.; Kevrekidis, I. G.; Saville, D. A.; Aksay, I. A. J. Appl. Phys. 2012, 112, 074905.
(16) Genshaw, M. A.; Damjanov., A.; Bockris, J. O. J. Electroanal. Chem. 1967, 15, 163−172.
(17) Braun, M.; Nobe, K. J. Electrochem. Soc. 1979, 126, 1666−1671.
(18) Lee, H. P.; Nobe, K. J. Electrochem. Soc. 1986, 133, 2035−2043.
(19) Kear, G.; Barker, B. D.; Walsh, F. C. Corros. Sci. 2004, 46, 109−135.
(20) Solomentsev, Y.; Bohmer, M.; Anderson, J. L. Langmuir 1997, 13, 6058−6068.
(21) Ristenpart, W. D.; Aksay, I. A.; Saville, D. A. Langmuir 2007, 23, 4071−4080.
(22) Levich, V. G. In Physicochemical Hydrodynamics; Prentice-Hall, Inc.: Englewood Cliffs, NJ, 1962.
(23) Prieve, D. C.; Anderson, J. L.; Ebel, J. P.; Lowell, M. E. J. Fluid Mech. 1984, 148, 247−269.
(24) Punckt, C.; Aksay, I. A. J. Chem. Phys. 2009, 131, 244710.
(25) Hunter, R. J. In Zeta Potential in Colloid Science; Academic Press, Inc.: New York, 1981.
(26) O'Brien, R. W.; White, L. R. J. Chem. Soc., Faraday Trans. 2 1978, 74, 1607−1626.
(27) Murira, C. M.; Punckt, C.; Schniepp, H. C.; Khusid, B.; Aksay, I. A. Langmuir 2008, 24, 14269−14275.
(28) West, J. M. In Basic Corrosion and Oxidation; Ellis Horwood Ltd.: West Sussex, England, 1986.
(29) Aoki, K. Electroanalysis 1993, 5, 627−639.
(30) Ibl, N. Electrodics: Transport. In Comprehensive Treatise of Electrochemistry; Yeager, E., Bockris, J. O'M., Conway, B. E., Sarangapani, S., Eds.; Plenum Press: New York, 1983; Vol. 6.
(31) Newman, J.; Thomas-Alyea, K. E. In Electrochemical Systems; John Wiley & Sons, Inc.: Hoboken, NJ, 2004.
(32) Bard, A. J.; Faulkner, L. R. In Electrochemistry; John Wiley & Sons: New York, 1980.
(33) Smyrl, W. H. J. Electrochem. Soc. 1985, 132, 1555−1562.

(34) Oldham, K. B. *J. Electroanal. Chem.* **1981**, *122*, 1−17.

(35) Moran, J. L.; Posner, J. D. *J. Fluid Mech.* **2011**, *680*, 31−66.

(36) Dukhin, S. S.; Derjaguin, B. V. In *Electrophoresis*; Nauka: Moscow, 1976.

(37) Rubinstein, I.; Zaltzman, B. *Math. Models Methods Appl. Sci.* **2001**, *11*, 263−300.